Grain Growth Control of ZnO-V2O5-Cr2O3 Based Varistors by PrMnO3 Addition

Chankun Cai
Inner Mongolia University of Science and Technology
Yu Shi
Inner Mongolia University of Science and Technology
Manyi Xie
Inner Mongolia University of Science and Technology
Ke Xue
Inner Mongolia University of Science and Technology
Maofeng Xu
Inner Mongolia University of Science and Technology
Yanlong Wu
Inner Mongolia University of Science and Technology
Jun Peng
Inner Mongolia University of Science and Technology
Shengli An (shengli_an@126.com)

Research Article

Keywords: Abnormal grain growth, ZnO, V2O5, Varistor

Posted Date: October 26th, 2021

DOI: https://doi.org/10.21203/rs.3.rs-968568/v1

Grain growth control of ZnO-V_2O_5-Cr_2O_3 based varistors by $PrMnO_3$ addition

Changkun Cai [a, b], Yu Shi [a], Manyi Xie [a, b], Ke Xue [a, b], Maofeng Xu [a, b], Yanlong Wu [a], Jun Peng [a, b], Shengli An [a, b*]

[a] School of Materials and Metallurgy, Inner Mongolia University of Science and Technology, Baotou 014010, China

[b] Inner Mongolia Key Laboratory of Advanced Ceramic Materials and Devices, Inner Mongolia University of Science and Technology, Baotou 014010, China

* Corresponding authors: Shengli An: shengli_an@126.com

Abstract

In this work, the grain growth behaviour of ZnO+V_2O_5(1 mol%)+Cr_2O_3(0.35 mol%)-based ceramics with 0.25–0.75 mol% additions of $PrMnO_3$ was systematically investigated during sintering from 850°C to 925°C with the aim to control the ZnO grain size for their application as varistors. It was found that with the increased addition of $PrMnO_3$, not only did the average grain size decrease, but the grain size distribution also narrowed and eventually changed from a bimodal to unimodal distribution after a 0.75 mol% $PrMnO_3$ addition. The grain growth control was achieved by a pinning effect of the secondary $ZnCr_2O_4$ and $PrVO_4$ phases at the ZnO grain boundaries. The apparent activation energy of the ZnO grain growth in these ceramics was found to increase with increased additions of $PrVO_4$; hence, the observed reduction in the ZnO grain sizes.

***Keywords*:** Abnormal grain growth; ZnO; V_2O_5; Varistor

1. Introduction

ZnO-Bi_2O_3 ceramics are an established class of ZnO-based varistors. It is well known that the nonlinear current-voltage (*I–V*) characteristics of these ZnO-Bi_2O_3 varistors are directly dependent on their microstructures, mainly the average grain size and size distribution of ZnO. Typically, a large average grain size of >30 μm is required for low-voltage applications, and a small average grain size of <10 μm is needed for high-voltage applications [1]. Additionally, a narrow grain size distribution is also critical for achieving stability of the electrical field strength of these materials [2].

It has been found that ZnO-V_2O_5 ceramics also exhibit a nonlinear *I–V* behaviour comparable to ZnO-Bi_2O_3 ceramics [3, 4] and thus have the potential to be a new class of varistors. One of the significant advantages of ZnO-V_2O_5 ceramics is that they can be sintered at a relatively low temperature of ~900°C [3-6]. This outstanding feature allows these ceramics to be co-fired with Ag (m.p. 961°C). This enables Ag, instead of expensive Pd or Pt, to be used as inner electrodes for applications in multilayer chip components [7]. Moreover, V_2O_5 is also a better sintering aid compared to Bi_2O_3 for ZnO, enabling ZnO-V_2O_5-based ceramics to be densified to the same density at a lower temperature than ZnO-Bi_2O_3-based ceramics [8, 9].

However, ZnO-V_2O_5-based ceramics suffer from a distinct disadvantage in that they have been shown to exhibit abnormal ZnO grain growth [10, 11]. This is commonly attributed to the high reactivity of the V_2O_5-rich liquid phase formed during sintering. This phase assists in the diffusion of Zn^{2+} and thus promotes ZnO grain growth, which results in the formation of abnormally grown grains (AGG) of ZnO.

One approach to curb the formation of AGG in ZnO-V_2O_5 ceramics is to induce the formation of a secondary phase to hinder ZnO grain growth by the addition of a third oxide to the system [12, 13]. The two commonly used additives are Cr_2O_3 and Sb_2O_3, as Cr_2O_3 can react with ZnO to form a $ZnCr_2O_4$ spinel phase, while Sb_2O_3 and ZnO form spinel phases of $ZnSb_2O_6$ and $Zn_{2.33}Sb_{0.67}O_4$ [12-14]. However, these two additives have their own specific limitations. With Cr_2O_3, an addition greater than 1 mol% is required to effectively counter the AGG and refine the ZnO grain size in ZnO-V_2O_5 ceramics [13]. However, at this required addition level, Cr_2O_3 has also been found to segregate at grain-boundary regions, leading to the deterioration of *I–V* behaviour due to high leakage current [12]. With Sb_2O_3, an addition of up to 2 mol% is needed to control the grain growth of ZnO-V_2O_5; however, the addition of Sb_2O_3 increases the required sintering temperature for the system. At an Sb_2O_3 content greater than 0.5 mol%, the sintering temperature could increase to 1200°C [13], nullifying the advantage of having the ZnO-V_2O_5-based system in the first place.

This work investigated the effect of $PrMnO_3$ addition on the grain growth of ZnO-V_2O_5-Cr_2O_3 ceramics with the aim to control the average grain size and size distribution of ZnO to improve their electrical properties as practical varistors.

2. Experimental

2.1 Sample preparation

All the reagents used in this work were of analytical grade (>99.5% purity) and were supplied by SINOPHARM. $PrMnO_3$ powder was prepared in-house by mixing Pr_6O_{11} and $MnCO_3$ at a molar ratio of 1:6 and allowing the mixture to react at 1000°C for 5 h in air. The formation of $PrMnO_3$ phase was confirmed by X-ray powder diffraction (XRD) analysis.

Table 1 summarises the nominal compositions of constituent powders used to prepare four ZnO-V_2O_5-Cr_2O_3 ceramic samples and their designated sample names. The $PrMnO_3$ powder was introduced with the aim to regulate the grain growth in these ceramics.

Table 1. Basic compositions of the ZnO ceramics studied in this work

Sample Name	Nominal Powder Compositions
ZVC	ZnO+V_2O_5(1 mol%)+Cr_2O_3(0.35 mol%)
ZVCP25	ZnO+V_2O_5(1 mol%)+Cr_2O_3(0.35 mol%)+$PrMnO_3$(0.25 mol%)
ZVCP50	ZnO+V_2O_5(1 mol%)+Cr_2O_3(0.35 mol%)+$PrMnO_3$(0.50 mol%)
ZVCP75	ZnO+V_2O_5(1 mol%)+Cr_2O_3(0.35 mol%)+$PrMnO_3$(0.75 mol%)

For each nominal composition, the powder mixture was homogenized by ball milling in absolute alcohol using zirconia balls in a polypropylene container on a planetary mill for 24 h. After milling, the powder mixture was dried at 80°C for 24 h. The dried powder mixture was then mixed with 5 wt% polyvinyl alcohol (PVA) binder and pressed into pellets of Φ12 mm × 1 mm under a uniaxial pressure of 130 MPa. The green pellets were first fired at 500°C for 1 h to remove the binder before being subjected to different sintering temperature/time regimes in an alumina crucible at a heating rate of 4°C/min. In this work, seven sintered ceramic discs for each nominal composition were produced at 850°C, 900°C, and 925°C for 4 h and at 875°C for 2, 4, 6, and 8 h. After sintering, the furnace was powered off to allow the sintered discs to cool down naturally within the furnace.

2.2 Sample characterization

The phase compositions of the sintered and quenched samples were analysed by XRD

patterns obtained using a diffractometer (PANalytical X'pert Powder) with Cu $K_{\alpha 1}$ radiation ($\lambda = 0.1541$ nm).

The microstructure of the sintered samples was observed and analysed by scanning electron microscopy (SEM) using a ZEISS Supra 55 electron microscope. A polished cross-sectional area along the thickness of the sintered disc was prepared and chemically etched in a dilute HCl solution to reveal the grain and phase structures for SEM observation.

The average ZnO grain size and grain size distribution were analysed using a representative SEM image of each sintered sample.

To determine the average grain size, the method reported by Mendelson [16] was used. Basically, the average grain-boundary intercept length ($\bar{L}$) was first determined by measuring along 10 randomly drawn lines across the SEM image. The average grain size G is then calculated by Eq. (1):

$$G = 1.56\bar{L}. \qquad (1)$$

To determine the ZnO grain size distribution, the dimensions around 500–800 ZnO grains of each sample were measured from its SEM images using a dedicated image analysis software. The surface area (S) of each grain was then estimated, and the equivalent diameter (d) of each grain was obtained by transforming the surface area of the irregularly shaped grain into a circle of the same area using the method reported by Daneu [17].

The grain growth behaviour was analysed using a phenomenological kinetic grain growth equation established by Nicholson et al. [18], which has been widely used for ZnO-based ceramic systems [8, 10, 18, 19]. The equation is expressed as follows:

$$G^n - G_0^n = K_0 t \exp\left(\frac{-Q}{RT}\right), \qquad (2)$$

where G is the average grain size of the ZnO ceramic at time t, G_0 is the initial grain size of the ZnO powder, n is the kinetic grain growth exponent, Q is the apparent activation energy, R is the universal gas constant, T is the absolute temperature, and K_0 is a T-independent constant. In the case where G_0 is significantly smaller than G, then Eq. (2) is simplified to

$$G^n = K_0 t \exp\left(\frac{-Q}{RT}\right). \qquad (3)$$

Equation (3) was used throughout this study to analyse the sintering behaviour of the

ZnO-V_2O_5-Cr_2O_3 samples studied in this work.

2.3 Sample I-V characteristics

The DC current-voltage (I–V) behaviour of the sintered samples was measured using a withstand voltage tester (MS2671A, Xi'an Instruments Inc., China). The sintered discs (~Φ8 mm × 1 mm thickness) were painted with a silver paste on both surfaces to enable the measurements. The $I-V$ curve was determined by measuring the current at a stepwise-increased applied voltage until I reached 10 mA. The field strength (E) is defined as the applied voltage per sample thickness, and the current density (J) is the measured current per sample area. The switching field strength $E_{1\ mA/cm^2}$ is the field strength at J=1 mA·cm^{-2}. The nonlinear coefficient (α) is calculated by Eq. (4):

$$\alpha = \frac{1}{lgE_{10mA/cm^2} - lgE_{1mA/cm^2}}$$

where $E_{10\ mA\cdot cm^{-2}}$ and $E_{1\ mA\cdot cm^{-2}}$ are the field strengths at 10 mA·cm^{-2} and 1 mA·cm^{-2}, respectively. The higher the value of α is, the better it is for a varistor.

3. Results and Discussion

3.1 Phase compositions and distributions in sintered samples

Fig. 1 shows the XRD patterns of the four ZVCP samples sintered at 875 °C for 4 h. For the ZVC sample, in addition to the main ZnO phase, several minor phases were also detected, including $Zn_4V_2O_9$, α-$Zn_3(VO_4)_2$, and $ZnCr_2O_4$. These minor phases have been commonly observed and reported in sintered ZnO-V_2O_5-Cr_2O_3 systems [12]. With the addition of $PrMnO_3$, a new minor phase of $PrVO_4$ was also observed in the ZVCP25, ZVCP50, and ZVCP75 samples.

The formation of the $PrVO_4$ phase is believed to resulte from the reaction between α-$Zn_3(VO_4)_2$ and $PrMnO_3$ during sintering following the reaction:

$$\alpha\text{-}Zn_3\left(VO_4\right)_2 + 2\,PrMnO_3 \longrightarrow 2\,PrVO_4 + Mn_2O_3 + 3ZnO$$

This has also been reported by Zhao et al. [20].

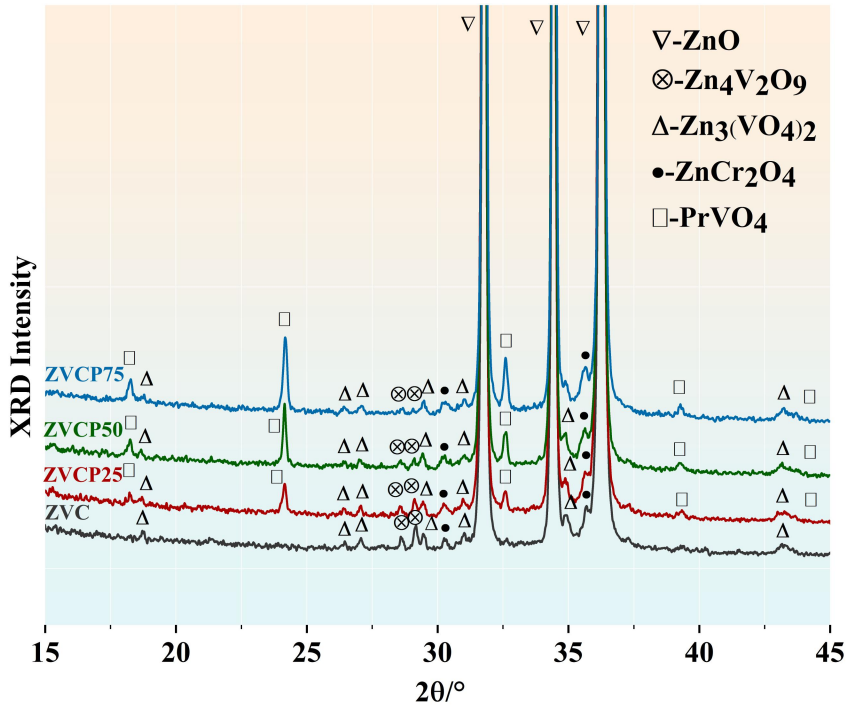

Fig. 1. XRD patterns of the ZVC, ZVCP25, ZVCP50, and ZVCP75 samples sintered at 875 °C for 4 h.

Fig. 2 shows a typical microstructure of a sintered ZVCP50 sample. As expected, the dominant morphology included grains of the ZnO phase, and the focus here was on the appearance and distribution of the minor phases. As seen in the micrograph, in addition to $ZnCr_2O_4$ (ZC) clusters (circled in white-dashed lines), $PrVO_4$ (PV) grains (circled in yellow-dashed lines) were clearly seen to also distribute at the junctions of ZnO grains. In some cases, ZnO grains were observed to grow around either $ZnCr_2O_4$ clusters or $PrVO_4$ grains. Fig. 3 shows the TEM image reveal the difference in microstructure between the second phase particles $PrVO_4$ and $ZnCr_2O_4$. The electron diffraction pattern in Fig. 3 further confirmed the existence of $PrVO_4$ and $ZnCr_2O_4$. The $ZnCr_2O_4$ grains are very small that the grain size is below 0.2 μm, but the $PrVO_4$ grains have a relatively larger size than $ZnCr_2O_4$ which ranges from 0.5μm to 4μm. Most grains of $ZnCr_2O_4$ and $PrVO_4$ were found located at the ZnO grain boundaries, and $ZnCr_2O_4$ grains tend to aggregate to form a heap of ~ 1μm in size. This observation suggests that these secondary minor phases could exert a 'pinning' effect, which hindered the movement of the grain boundaries of ZnO, thus limiting its grain growth.

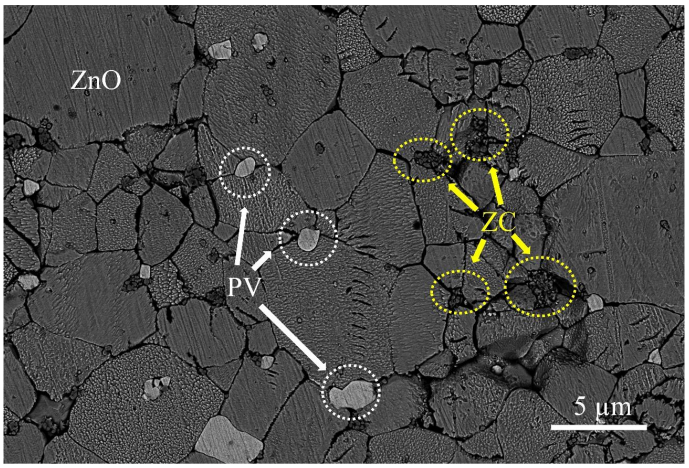

Fig. 2. Back-scattered electron (BSE) image of a ZVCP50 sample sintered at 875°C for 4 h.

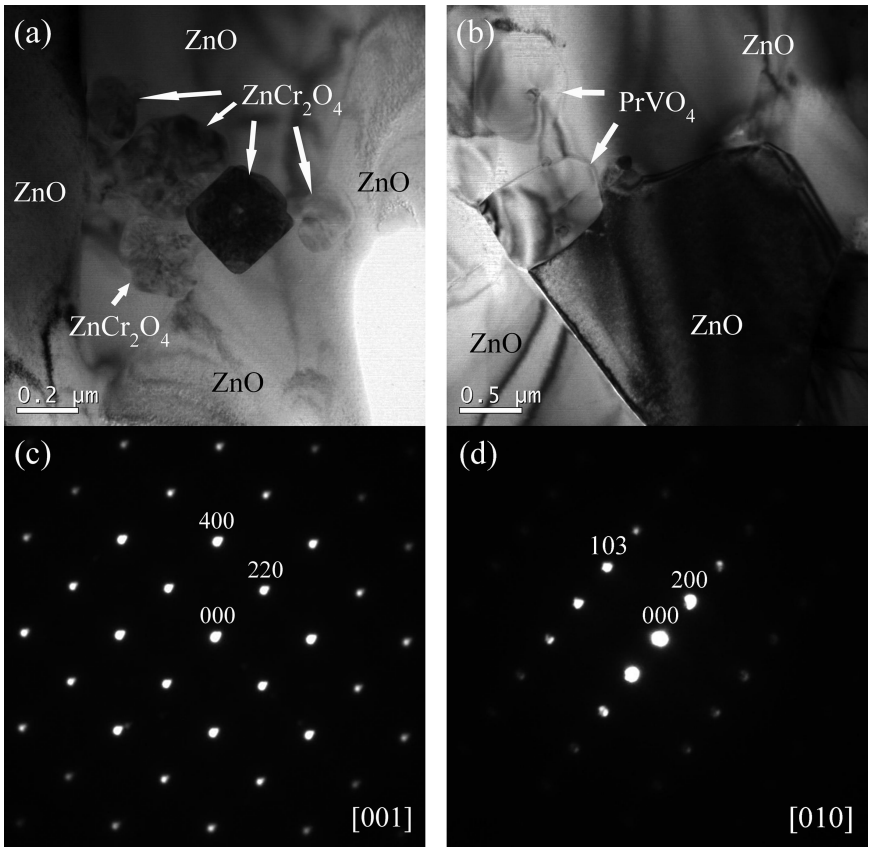

Fig. 3. TEM micrographs and electron diffraction patterns from secondary particle grains: (a) bright-field image of $ZnCr_2O_4$ grains from a sample with the composition of ZVCP75 sintered at 875 °C for 4 h, (b) bright-field image of $PrVO_4$ grains from a sample with the composition of ZVCP75 sintered at 875 °C for 4 h, (c) electron diffraction pattern from the [001] zone of $ZnCr_2O_4$ grain in (a) and (d) electron diffraction pattern from the [010] zone of $PrVO_4$ grain in (b).

3.2. Average ZnO grain sizes in sintered samples

For all fours sintered samples, the average grain size of each sample under all sintering conditions was determined following the procedure described in 2.2, and the results are summarized in Table 2.

Table 2. Average grain sizes estimated from SEM analysis of ZVC and ZVCP samples sintered at different conditions

Sample	Average grain size, G (μm)						
	850°C 4 h	900°C 4 h	925°C 4 h	875°C 2 h	875°C 4 h	875°C 6 h	875°C 8 h
ZVC	6.55	9.42	10.55	4.15	5.19	6.04	6.68
ZVCP25	4.95	7.14	9.65	3.18	3.94	4.62	4.8
ZVCP50	4.05	6.81	7.69	2.93	3.81	4.00	4.32
ZVCP75	3.02	5.04	6.76	2.47	2.80	2.95	3.14

3.3. Kinetic grain growth parameters

To reveal the effect of $PrMnO_3$ addition on the sintering behaviour of the ZnO-V_2O_5-Cr_2O_3 ceramics, the isothermal grain growth behaviour at 875°C was first analysed using a rearranged Eq. (3), as shown below:

$$\log G = \frac{1}{n}\log t + \frac{1}{n}\left[\log K_0 - 0.434\left(\frac{Q}{RT}\right)\right]. \qquad (4)$$

Figure 4 illustrates $logG$ vs. $logt$ curves, which show the isothermal grain growth behaviour of the four samples sintered at 875°C for 2–8 h. A linear fit of the curves enabled the determination of the kinetic grain growth exponent n from the slope of the linear fit for each sample. The n values so determined are also shown in Fig. 4. Notably, with the increased addition of $PrMnO_3$, not only did the average grain size G decrease, the grain growth rate also decreased, as indicated by the increased n values.

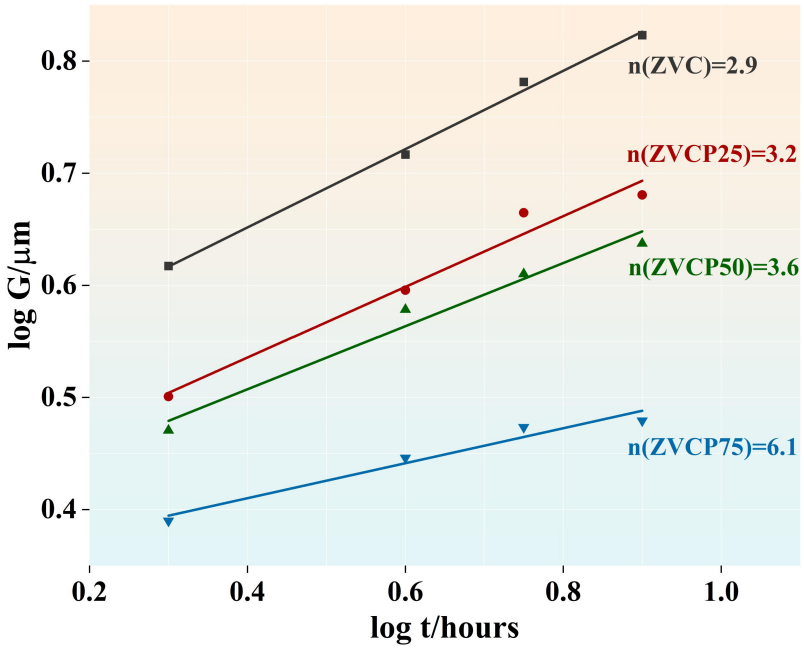

Fig. 4. Grain growth behaviour of the four samples sintered at 875 °C for 2-8 hours.

To determine the apparent activation energy Q associated with the grain growth, Eq. (3) is rearranged as

$$\log\left(\frac{G^n}{t}\right) = \log K_0 - \frac{0.434Q}{R}\left(\frac{1}{T}\right) \qquad (5)$$

Q can then be calculated from the gradient of the Arrhenius plot of $\log(G^n/t)$ vs. $(1/T)$. Figure 5 shows the Arrhenius plots of the four samples from the G values obtained at different sintering temperatures shown in Table 2. The apparent activation energy Q values determined from Fig. 5 are summarized in Table 3, together with the n values determined from Fig. 4.

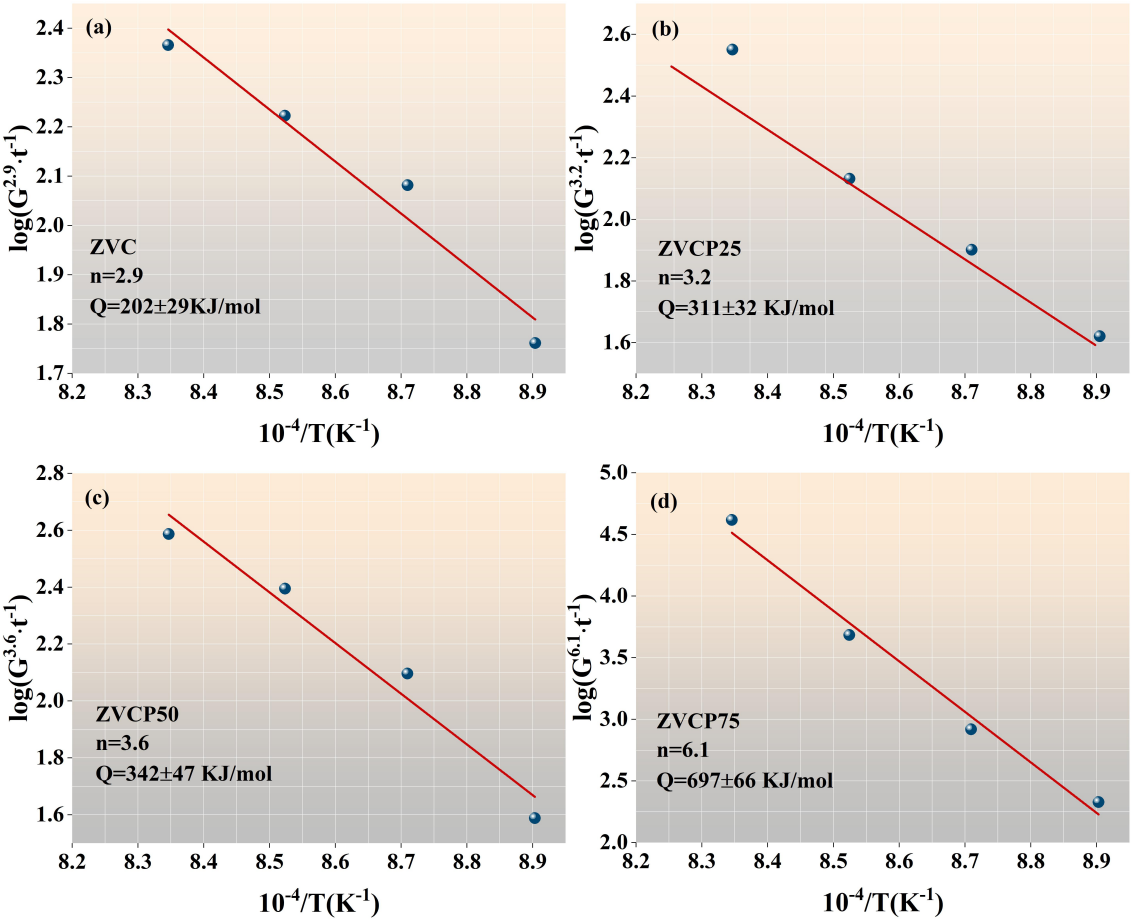

Fig. 5. The $\log(G^n/t)$ vs. $(1/T)$ Arrhenius plots for grain growth of the four sintered samples: (a) ZVC, (b) ZVCP25, (c) ZVCP50, and (d) ZVCP75.

Table 3. Summary of ZnO grain growth exponents and apparent activation energy for grain growth

Ref	Material system (nominal composition, mol%)	Sintering temperature T (°C)	Growth exponent n	Apparent activation energy Q (kJ/mol)
[22]	Pure ZnO	900–1400	3.0	224±16
[28]	ZnO-V_2O_5(0.5-2.0)	900–1200	1.5–1.8	~88
[2]	ZnO-V_2O_5(0.5-2.0)	900	1.2–1.6	–
[29]	ZnO-V_2O_5(1.0)	750–1200	1.4	76±7
[14]	ZnO-V_2O_5(0.5)-Sb_2O_3(0.5)	900–1050	4.0	365
This study	ZnO+V_2O_5(1.0)+Cr_2O_3(0.35)	875	2.9	202±29
	ZnO+V_2O_5(1.0)+Cr_2O_3(0.35)+$PrMnO_3$(0.25)	875	3.2	311±32
	ZnO+V_2O_5(1.0)+Cr_2O_3(0.35)+$PrMnO_3$(0.50)	875	3.6	342±47
	ZnO+V_2O_5(1.0)+Cr_2O_3(0.35)+$PrMnO_3$(0.75)	875	6.1	697±66

As seen in Table 3, from both of this work and other published works, the basic

ZnO-V_2O_5 binary systems had a kinetic grain growth exponent n value spanning 1.5–1.8. This n value was lower than the $n = 3.0$ observed for pure ZnO, indicating that the addition of V_2O_5 encouraged the grain growth of ZnO. This was attributed to the high reactivity of the V_2O_5-rich liquid phase during sintering, promoting the formation of abnormally grown ZnO grains.

The addition of a third component—e.g., the 0.35 mol% of Cr_2O_3 in this study or 0.5 mol% Sb_2O_3 as reported elsewhere[21]—has been shown to increase the n value to 2.9 and 4.0, respectively. This means that the addition of a third component could hinder ZnO grain growth in basic ZnO-V_2O_5 binary systems. In both cases, this was attributed to the formation of spinel $ZnCr_2O_4$ or a $ZnSb_2O_4$ secondary phase, which exerts a pinning effect on ZnO grain boundaries and thus hinders ZnO grain growth [13, 21, 22].

It was clear that the addition of $PrMnO_3$ to the ZnO+V_2O_5 (1 mol%) + Cr_2O_3 (0.35 mol%) ceramics resulted in a further increase in the *n* value, which increased to 6.1 after a nominal addition of 0.75 mol% of $PrMnO_3$ for ZVCP75, demonstrating the high effectiveness of $PrMnO_3$ in suppressing ZnO grain growth. As seen in the XRD and SEM analyses, the addition of $PrMnO_3$ resulted in the formation of an additional spinel $PrVO_4$ phase, which was also found to be distributed at the grain boundaries of ZnO similarly to $ZnCr_2O_4$ in the sintered ceramics. A similar pinning effect was thus believed to be the main reason for the hindered ZnO grain growth by the addition of $PrMnO_3$.

As expected, it is clearly seen in Table 3 that the apparent activation energy values for the grain growth followed an inverse behaviour compared to the n values. Obviously, the higher the activation energy, the higher the n values, the slower the grain growth rate, and the smaller the average ZnO grain sizes.

3.4. Grain size distribution in sintered samples

Figure 6 shows SEM images and grain size distribution histograms of the four samples sintered at 875°C for 4 h. It was clear from the SEM images that with increased additions of $PrMnO_3$, not only did the average grain size of ZnO decrease, but the size distribution also narrowed significantly.

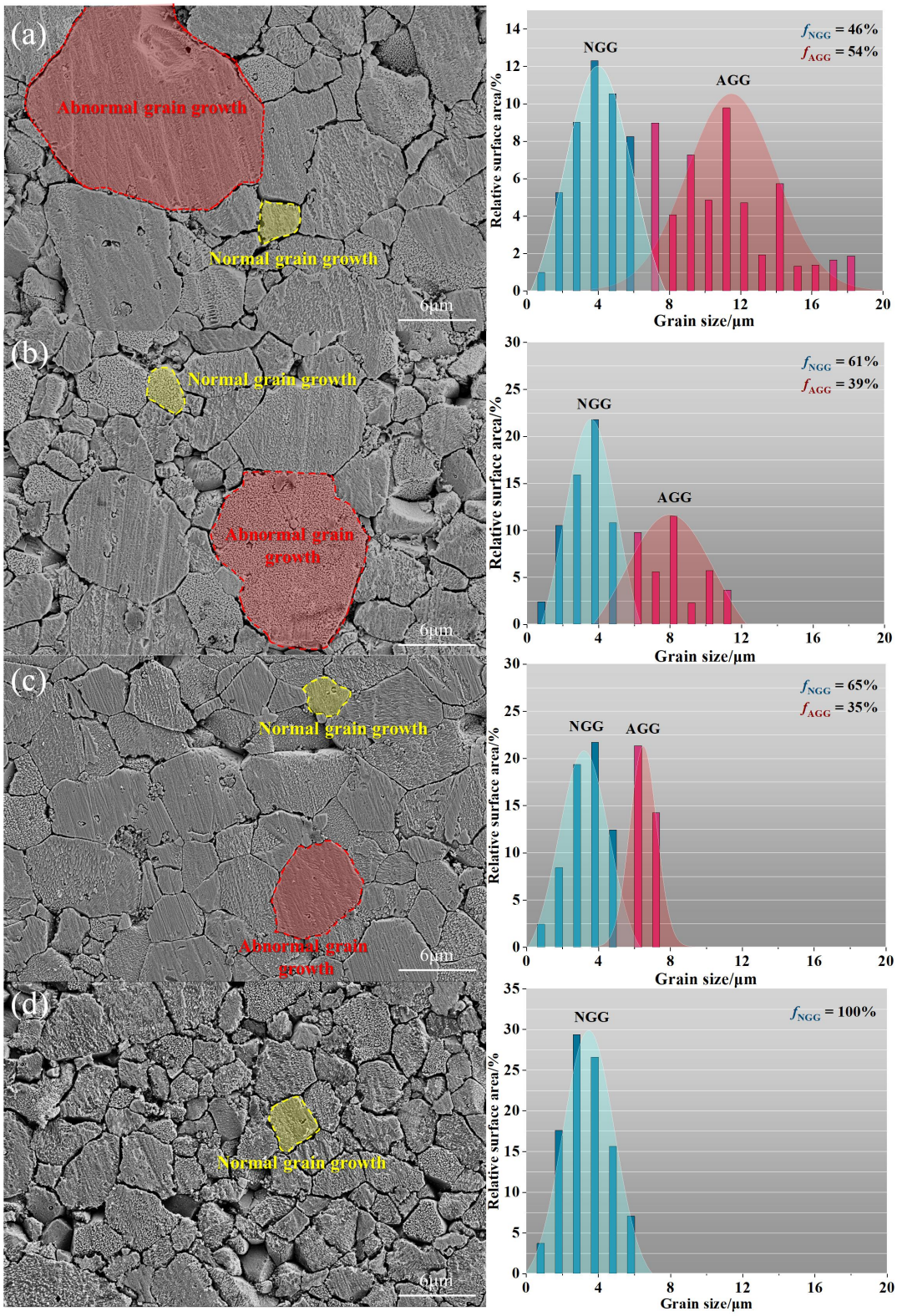

Fig. 6. SEM microstructures and grain size distribution histograms of the samples sintered at 875 °C for 4 h: (a) ZVC, (b) ZVCP25, (c) ZVCP50, and (d) ZVCP75. NGG and f_{NGG}refers to the normally grown grain and its number fraction. AGG and f_{AGG} refer to the abnormally grown grain and its number fraction.

Obviously, the ZVC sample without the addition of $PrMnO_3$ exhibited a broad and obviously bimodal grain size distribution. In the context of this work, larger grains are considered to be the AGG, and the relatively smaller grains are considered as the normally grown grains (NGG). The area fractions of AGG and NGG for each sample are also included in the size distribution histograms in the figure. The addition of $PrMnO_3$ not only resulted in the reduction and narrowing of the grain size range, but also a diminishing of the bimodal distribution. For ZVCP75, the grain size distribution became unimodal.

Figure 7 shows the average grain sizes of the AGG and NGG vs. the nominal addition of $PrMnO_3$. This revealed the impact of $PrMnO_3$ addition. Notably, the average grain size of NGG did not change much; however, the average grain size of the AGG decreased dramatically. This indicated the effectiveness of $PrMnO_3$ addition in suppressing the coarsening of ZnO grains in this system. The number fractions of AGG (f_{AGG}) and NGG (f_{NGG}) were also determined for the sintered samples and are provided in the histograms.

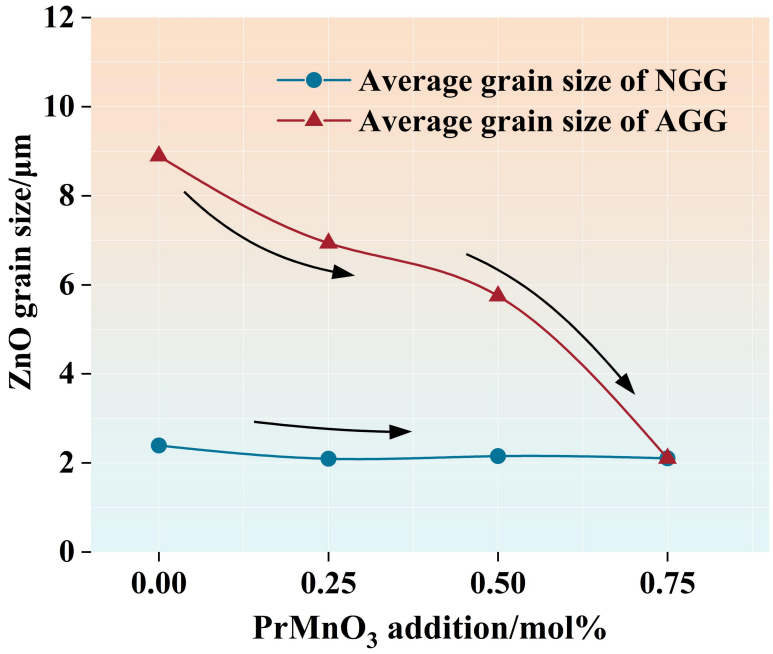

Fig. 7. Effect of nominal addition of $PrMnO_3$ on the average grain sizes of the AGG and NGG in ZVCP samples sintered at 875 °C for 4 h.

3.5. Electrical behaviour of sintered samples

Figure 8 shows the switching field strength $E_{1\,mA\cdot cm^{-2}}$ of the four samples sintered at 875°C for 4 h. For each sample, 10 specimens were prepared, their *I–V* curves were measured, and their $E_{1\,mA\cdot cm^{-2}}$ values were determined. Figure 8(a) shows all measured $E_{1\,mA\cdot cm^{-2}}$ data for the four samples. As seen, the basic ZVC sample displayed a very broad range of $E_{1\,mA\cdot cm^{-2}}$. Obviously, a 0.25 mol% nominal addition of $PrMnO_3$ resulted in a remarkable narrowing of the $E_{1\,mA\cdot cm^{-2}}$ range for the ZVCP25 sample. Further increasing the $PrMnO_3$ addition to 0.75 mol% produced a continuous narrowing of the $E_{1\,mA\cdot cm^{-2}}$ range.

This significant stabilization of the switching field strength was attributed to the uniformization of the ZnO grain size as the result of $PrMnO_3$ addition. As seen in Fig. 6, a 0.75 mol% addition of $PrMnO_3$ in ZVC effectively eliminated the formation of abnormally grown ZnO grains. The resulting ZVCP75 sample was shown to have a markedly improved stability in its switching field strength. This was also consistent with the results reported by Hng et al. [12], which showed that the presence of just a few abnormally grown ZnO grains could have a pronounced destabilization effect on the switching field strength of ZnO-V_2O_5 varistors.

Furthermore, with a 0.75 mol% addition of $PrMnO_3$, there was also an marked increase in the $E_{1\,mA\cdot cm^{-2}}$ value for the ZVCP75 sample. This increase in switch field strength was mostly due to the refined ZnO grain size.

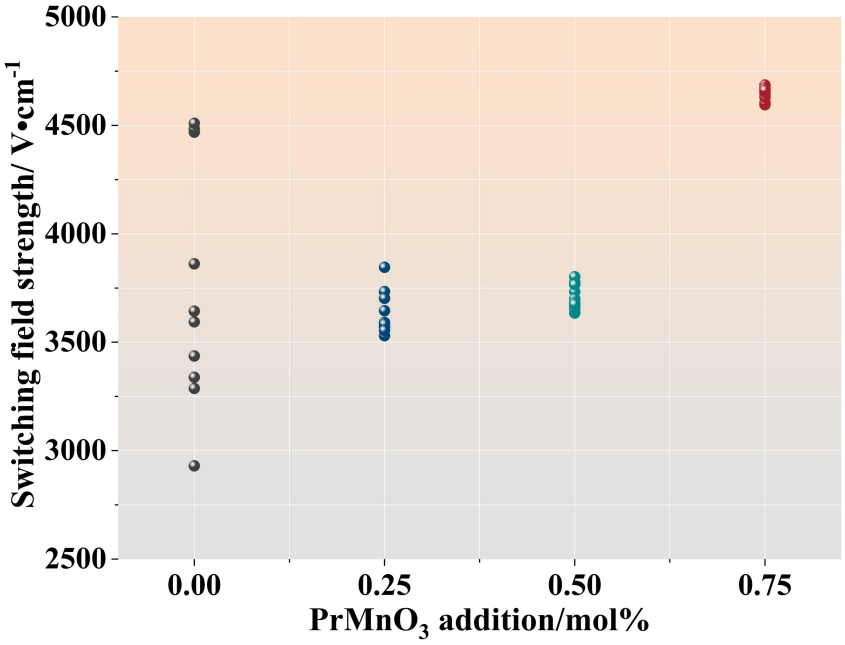

Fig. 8. Measured switching field strength data vs nominal addition amount of $PrMnO_3$.

Table 4 summarises the relative density and number fraction of AGG and the average grain size of the sintered samples, together with the nonlinear coefficient and the average and range of the switching field strength of these samples.

Table 4. Relative density, number fraction of AGG and average grain size, and electrical properties of the sintered samples at 875 °C for 4 h.

Sample	Relative density (%)	f_{AGG} (%)	Average grain size (μm)	Nonlinear coefficient α	$E_{1\ mA\cdot cm^{-2}}$ (V/cm)	
					Range	Average
ZVC	95.1	8.83	5.19	7.2	1580	3649
ZVCP25	94.8	6.53	3.94	7.7	316	3632
ZVCP50	95.1	5.66	3.81	7.8	167	3726
ZVCP75	95.7	0	2.80	8.9	91	4620

It was noted that all the samples possessed a high sintering density at close to 95% of the theoretical density of ZnO. While the addition of $PrMnO_3$ had little effect on the sintering density, it effectively reduced and eliminated the fraction of AGG and progressively refined the grain sizes of the resulting ceramics.

The homogenization and reduction of ZnO grain size were attributed to the noticeably enhanced electrical properties of the ceramics, most significantly the stabilization of the switching field strength. The nonlinear coefficient also increased marginally from 7.2 to 8.9 from ZVC to ZVCP75, respectively, as seen in Table 4.

In summary, when a small amount of $PrMnO_3$ was added to the ZnO-V_2O_5 (1 mol%)-Cr_2O_3 (0.35 mol%) ceramics, an additional second phase, $PrVO_4$, formed in addition to the commonly existing $ZnCr_2O_4$. Both of these phases tended to locate at the ZnO grain boundaries, hindering ZnO grain growth. Unlike the randomly distributed $ZnCr_2O_4$ particles, the $PrVO_4$ particles seemed to selectively participate in the regions where abnormal ZnO grain growth would take place, thus effectively suppressing the AGG. This was believed to be due to the formation of $PrVO_4$ consuming V_2O_5, which would only occur in the V_2O_5-rich liquid phase. This weakened the fast

solution–precipitation process of the V_2O_5-rich liquid phase during sintering, thus demoting the abnormal ZnO grain growth.

5. Conclusions

In this study, the effect of $PrMnO_3$ addition (0.25 to 0.75 mol%) on the grain growth behaviour of ZnO-V_2O_5(1 mol%)-Cr_2O_3(0.35 mol%) ceramics was systematically investigated during sintering from 850°C to 925°C with the aim to refine the ZnO grain structure. The main findings were as follows.

(1) The addition of $PrMnO_3$ not only uniformized but also refined the ZnO grains in the resulting ceramics. At a 0.75 mol% $PrMnO_3$ addition, the bimodal grain size distribution was completely eliminated, and the average ZnO grain size was reduced by more than 45% compared to the sample without $PrMnO_3$ addition.
(2) The addition of $PrMnO_3$ resulted in remarkably improved stability of the switching field strength, narrowing its range of variation from 1580 V/cm (without $PrMnO_3$ addition) to only 91 V/cm (with 0.75 mol% $PrMnO_3$ addition). The homogenization and reduction of the ZnO grain sizes were responsible for the observed stabilization of the switching field strength.
(3) A phenomenological analysis of the ZnO grain growth kinetics showed that the kinetic grain growth exponent *n* increased from 2.9 without $PrMnO_3$ to 6.1 after a 0.75 mol% $PrMnO_3$ addition, corresponding to an increase in apparent activation energy from 202±29 to 697±66 kJ/mol, respectively.
(4) The formation of a $PrVO_4$ secondary phase as the result of $PrMnO_3$ addition was responsible for the grain growth behaviour observed. The $PrVO_4$ phase was found to mostly locate at the ZnO grain boundaries, thus hindering and eventually eliminating the abnormal growth of ZnO grains.

Acknowledgements

XRD, SEM, and TEM examinations were performed at the Center of Laboratory, Inner Mongolia University of Science and Technology. We thank LetPub (www.letpub.com) for its linguistic assistance during the preparation of this manuscript.

Conflicts of interest

The authors declare that they have no known competing financial interests or personal relationships that could have appeared to influence the work reported in this paper.

References

[1] Li ST, Liu FY, Li B, et al. Inhomogeneity of Grain Boundaries of ZnO Varistor. *Chinese Journal of Materials Research* 1997, **10**: 170-175.

[2] Nan CW, Clarke DR. Effect of Variations in Grain Size and Grain Boundary Barrier Heights on the Current-Voltage Characteristics of ZnO Varistors. *Journal of the American Ceramic Society* 1996, **79**: 3185-3192.

[3] Tsai JK, Wu TB. Nonohmic characteristics of ZnO-V_2O_5 ceramics. *Journal of Applied Physics* 1994, **76**: 4817-4822.

[4] Tsai J, Wu T. Microstructure and nonohmic properties of binary ZnO-V_2O_5 ceramics sintered at 900 °C. *Materials Letters* 1996, **26**: 199-203.

[5] Hng HH, Chan PL. Effects of MnO_2 doping in V_2O_5-doped ZnO varistor system. *Materials Chemistry and Physics* 2002, **75**: 61-66.

[6] Pfeiffer H, Knowles KM. Effects of vanadium and manganese concentrations on the composition, structure and electrical properties of ZnO-rich MnO_2-V_2O_5-ZnO varistors. *Journal of the European Ceramic Society* 2004, **24**: 1199-1203.

[7] Nahm CW. Microstructure and electrical properties of ZnO–V_2O_5–MnO_2–Co_3O_4–Dy_2O_3–Nb_2O_5-based varistors. *Journal of Alloys and Compounds* 2010, **490**: L52-L54.

[8] Senda T, Bradt RC. Grain Growth in Sintered ZnO and ZnO-Bi_2O_3 Ceramics, *Journal of the American Ceramic Society* 1990, **73**: 106-114.

[9] Hng HH, Knowles KM. Microstructure and Current–Voltage Characteristics of Multicomponent Vanadium-Doped Zinc Oxide Varistors. *Journal of the American Ceramic Society* 2000, **83**: 2455-2462.

[10] Hng HH, Halim L. Grain growth in sintered ZnO-1 mol% V_2O_5 ceramics. *Materials Letters* 2003, **57**: 1411-1416.

[11] Kurzawa M, Rychlowska-Himmel I, Bosacka M. Reinvestigation of Phase Equilibria in the V_2O_5–ZnO System. *Journal of thermal analysis and calorimetry* 2001, **64**: 1113-1119.

[12] Hng HH, Chan PL. Cr_2O_3 doping in ZnO-0.5 mol% V_2O_5 varistor ceramics. *CERAMICS INTERNATIONAL* 2009, **35**: 409-413.

[13] Zhao M, Shi Y, et al. Grain growth of ZnO-V_2O_5 based varistor ceramics with different antimony dopants. *Journal of the European Ceramic Society* 2011, **31**: 2331-2337.

[14]Lao Y, Kuo S, Tuan W. Effect of powder bed on the microstructure and electrical properties of Bi_2O_3- and Sb_2O_3-doped ZnO. Journal of Materials Science: Materials in Electronics 2009, **20**: 234-241.

[15] Rios PR. A theory for grain boundary pinning by particles. *Acta Metallurgica* 1987, **35**: 2805-2814.

[16] Mendelson MI. Average Grain Size in Polycrystalline Ceramics, *Journal of the American Ceramic Society* 1969, **52**: 443-446.

[17] Daneu N, Rečnik A, Bernik S. Grain-Growth Phenomena in ZnO Ceramics in the Presence of Inversion Boundaries. *Journal of the American Ceramic Society* 2011, **94**: 1619-1626.

[18] Nicholson GC. Grain Growth in Zinc Oxide. *Journal of the American Ceramic Society* 1965, **48**: 214-215.

[19] Yang SC, German RM. Grain Growth Kinetics in Liquid-Phase-Sintered Zinc Oxide–Barium Oxide Ceramics. *Journal of the American Ceramic Society* 1991, **74**: 3085-3090.

[20] Zhao M, Han J, et al. Microstructure and Non-linearity Characterization of ZnVTiO Based Varistor Ceramics Doped with $PrMnO_3$ Typed Precursor. *JOURANAL OF SYNTHETIC CRYSTALS* 2014, **43**: 2258-2264.

[21] Daneu N, Re V C Nik A, Bernik S. Grain Growth Control in Sb_2O_3-Doped Zinc Oxide. *Journal of the American Ceramic Society* 2003, **86**: 1379-1384.

[22] PIANARO SA, PEREIRA EC, BULHOES LOS. Effect of Cr_2O_3 on the electrical properties of multicomponent ZnO varistors at the pre-breakdown region. *Journal of materials science* 1995, **30**: 133-141.

Supplementary Files

This is a list of supplementary files associated with this preprint. Click to download.

- Highlights.docx